Calcium Measurements in Perfused Mouse Heart: Quantitating Fluorescence and Absorbance of Rhod-2 by Application of Photon Migration Theory

Congwu Du,*† Guy A. MacGowan,‡ Daniel L. Farkas,*§ and Alan P. Koretsky†¶

*Center for Light Microscope Imaging & Biotechnology, †Dept. of Biological Sciences, ¶Pittsburgh NMR Center for Biomedical Research, Carnegie Mellon University, Pittsburgh, Pennsylvania and ‡Cardiovascular Institute, §Dept. of Bioengineering, University of Pittsburgh, Pittsburgh, Pennsylvania 15213 USA

ABSTRACT Both theoretical and experimental results are presented for the quantitative detection of calcium transients in the perfused mouse heart loaded with the calcium-sensitive fluorescent dye Rhod-2. Analytical models are proposed to calculate both the reflected absorbance and fluorescence spectra detected from the mouse heart. These models allow correlation of the measured spectral intensities with the relative quantity of Rhod-2 in the heart and measurement of the changes in quantum yield of Rhod-2 upon binding calcium in the heart in which multiple scattering effects are predominant. Theoretical modeling and experimental results demonstrate that both reflected absorbance and fluorescence emission are attenuated linearly with Rhod-2 washout. According to this relation, a ratiometric method using fluorescence and absorbance is validated as a measure of the quantum yield of calcium-dependent fluorescence, enabling determination of the dynamics of cytosolic calcium in the perfused mouse heart. The feasibility of this approach is confirmed by experiments quantifying calcium transients in the perfused mouse heart stimulated at 8 Hz. The calculated cytosolic calcium concentrations are 368 ± 68 nM and 654 ± 164 nM in diastole and systole, respectively. Spectral distortions induced by tissue scattering and absorption and errors induced by the geometry of the detection optics in the calcium quantification are shown to be eliminated by using the ratio method. Methods to effectively minimize motion-induced artifacts and to monitor the oxygenation status of the whole perfused heart are also discussed.

GLOSSARY

Nomenclature of tissue optics

λ	Optical wavelength;
μ_a^λ	Optical absorption coefficient of tissue at λ;
$\mu_s'^\lambda$	Reduced scattering coefficient of tissue at λ;
μ_{eff}	Effective attenuation coefficient: $\mu_{eff} = [3\mu_a^\lambda(\mu_a^\lambda + \mu_s'^\lambda)]^{1/2}$;
δ_{eff}	Effective penetration depth: $\delta_{eff} = 1/\mu_{eff}$;
ψ	Photon fluence rate in tissue;
A^λ	Absorbance spectrum;
$A^{\lambda 1,\lambda 2}$	Differential absorbance between λ_1 and λ_2;
D	Light diffusion coefficient: $D \cong [3\mu_s'^\lambda]^{-1}$;
mfp'	Reduced mean free path: $mfp' = [\mu_a^\lambda + \mu_s'^\lambda]^{-1}$;
R	Diffuse reflectance from tissue;
S	Photon source in tissue.

Calculation of fluorescence

λ_x	Excitation wavelength;
λ_m	Emission wavelength;
μ_{af}^λ	Absorption coefficient of the fluorophore at λ;
$\Phi^{\lambda x,\lambda m}$	Fluorescence quantum efficiency/yield for emission at λ_m, given excitation at λ_x;
ψ_f	Fluorescence photon fluence rate;
$E^{\lambda m}$	Escape function (or probability) of fluorescent light;
$F^{\lambda x,\lambda m}$	Fluorescence intensity from tissue emitted at λ_m, when excited at λ_x;
$N^{\lambda x}$	Excitation photon density;
N_f	Fluorescent photon density;
$S^{\lambda m}$	Fluorescent source emitted at λ_m in tissue.

Calcium calculation and others

α_F	Deflection angle of detector off the normal direction of the incident beam;
Ω_F	Solid angle of optical detector;
B^λ	Background fluorescence emission at λ;
$[Ca^{2+}]_i$	Intracellular calcium concentration;
F	Calcium-dependent fluorescence intensity;
F/A	Ratio of fluorescence intensity over differential absorbance between excitation and detection wavelengths;
ΔF	Calcium-dependent fluorescence transients from diastole to systole;
G	Geometric factor of optical detection system: $G = \Omega_F/2\pi\cos\alpha_F$;
K_d	Rhod-2 dissociation constant for calcium;
Mn^{2+}	Manganese chloride mixed in perfusate.

INTRODUCTION

Cytosolic free calcium (Ca^{2+}) is an important regulator of cardiac metabolism and contractility. Fluorescence technol-

Received for publication 18 February 1999 and in final form 28 September 2000.

Address reprint requests to Dr. Congwu Du, Center for Light Microscopy Imaging and Biotechnology, 4400 Fifth Ave., Pittsburgh, PA 15213. Tel.: 412-268-6711; Fax: 412-268-6571; E-mail: congwu@andrew.cmu.edu.

Alan P. Koretsky's current address is NIH/NINDS, Bldg. 10, BID-69B, MSC 1060, 9000 Rockville Pike, Bethesda, MD 20892. Tel.: 301-402-9659; Fax: 301-402-0119; E-mail: koretskya@ninds.nih.gov.

0006-3495/01/01/549/13 $2.00

ogy has demonstrated significant potential for detection of Ca^{2+} transients in perfused hearts (Fralix et al., 1990; Brandes et al., 1992). Importantly, as most Ca^{2+} indicators have bright fluorescence emission, a minimal concentration of fluorescent dye is required for Ca^{2+} detection, thus minimizing the potentially toxic buffering effects of the calcium indicator on cardiac function.

Some of the calcium-sensitive fluorescent dyes, for instance, Fura-2 and Indo-1, have been used to quantitatively determine the concentration of intracellular calcium ($[Ca^{2+}]_i$) in biological tissues and the heart (Brandes et al., 1993; Haworth and Redon, 1998). These calcium indicators require fluorescence excitation in the ultraviolet (UV) range, where the overwhelming scattering and strong absorption of tissue substantially limits light penetration into tissue. This is of particular significance to $[Ca^{2+}]_i$ measurements in either the perfused heart or in vivo studies because the tissue scattering and absorption by myoglobin, cytochromes, and hemoglobin (in the presence of blood) restrict the detection of Ca^{2+}-dependent fluorescence light to only the outermost layers of the heart. In addition, changes in scattering and absorbance associated with different physiologic states are large in the UV range.

Recently, calcium indicators excitable by visible light, e.g., Rhod-2, have become commercially available. One advantage of these fluorescent dyes over the UV-excitable calcium indicators is a significant enhancement of fluorescence emission upon calcium binding. More importantly, both excitation and emission of the Ca^{2+}-dependent fluorescence are in the visible wavelength range, i.e., within the so-called "therapeutic window" (Parrish, 1981), where the relatively low absorption and the predominantly forward-directed scattering of tissue (Wilson and Patterson, 1986; Flock et al., 1987; Jacques et al., 1987) permits substantially increased penetration of the excitation light into the tissue and enhanced escape (i.e., remittance) of the fluorescent photons from tissue. In addition, the interference from autofluorescence in tissue is reduced in this wavelength region.

It has been known that multiple scattering effects of both excitation and emission light can perturb quantitative measurements of fluorescence calcium indicators (Brandes et al., 1994). The conventional methods using dual-wavelength fluorescence excitation or emission for ratio measurements have been used to extract $[Ca^{2+}]_i$ based on a spectral shift in either the excitation or emission spectrum upon binding Ca^{2+} (Grykiewicz et al., 1985; Brandes et al., 1993; Field et al., 1994). This fluorescence ratio technique can eliminate the influence of dye concentration change and minimize the errors induced by tissue scattering, tissue absorption, and motion artifacts (Koretsky et al., 1987; Fralix et al., 1990; Brandes et al., 1992). However, many of the visible light-excited calcium fluorescence dyes that are readily available do not exhibit a spectral shift upon calcium binding (Haugland, 1996). For example, Fig. 1 shows the

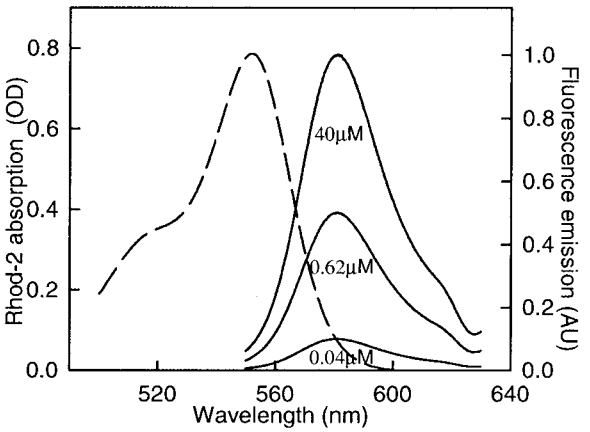

FIGURE 1 Absorption (*dashed curve*) and Ca^{2+}-dependent fluorescence (*solid curves*) spectra of Rhod-2 (10 μM) in solutions with various Ca^{2+} concentrations (0.04–40 μM).

absorption and fluorescence emission spectra of Rhod-2 (10 μM) in aqueous solution with various Ca^{2+} concentrations (0.04–40 μM). It is clear that increasing the Ca^{2+} concentration only causes an increase of the fluorescence intensity, and no spectral shift in excitation and emission. This precludes the use of the conventional fluorescence ratiometry mentioned above, thus making the quantification of $[Ca^{2+}]_i$ using Rhod-2 a challenging problem.

To enable the use of Rhod-2 as a calcium indicator in perfused hearts, Del Nido et al. (1998) proposed an empirical approach to quantify the concentration of Rhod-2 in perfused rabbit heart by measuring the reflected absorbance. This approach was based on the finding that the ratio of the fluorescence to absorbance was unchanged with the concentration change of Rhod-2 in the heart; thus the fluorescence-to-absorbance ratio was used to measure the change in the quantum yield of Rhod-2 with changes in $[Ca^{2+}]_i$ in the perfused rabbit heart. Substantial work needs to be done both theoretically and experimentally to validate this method, particularly in the presence of tissue scattering. Also, the possible spectral distortions caused by the interplay of factors such as tissue scattering, absorption, and the detection geometry, as well as their impact on quantitation accuracy, need to be further investigated.

In this study we extend the Rhod-2-based Ca^{2+} measurement to the perfused mouse heart. To systematically analyze the influence of tissue optical properties (e.g., scattering and absorption) on $[Ca^{2+}]_i$ determination, analytical models for the absorbance and fluorescence spectra are derived within the framework of photon diffusion theory. Our model predicts a proportional decay of the fluorescence and absorbance intensities as a result of Rhod-2 washout, thus verifying that the fluorescence-to-absorbance ratio can be used to compensate for the influence of the Rhod-2 concentration changes on $[Ca^{2+}]_i$ measurement in the heart. Moreover, we demonstrate that the fluorescence-to-absorbance ratio as a

measure of quantum yield in the $[Ca^{2+}]_i$ calculation can eliminate the distortions induced by tissue optical properties and geometrical complications. The results of our modeling are confirmed by experiments with Rhod-2 infusion into the perfused mouse heart.

THEORY

The mouse heart, like most biological tissue, has marked light-scattering properties. The light incident into it will undergo not only absorption, but also multiple scattering events; a quantitative analysis of the detected optical signal from an illuminated, perfused mouse heart is very complicated. This is because both fluorescence excitation and emission will involve photon diffusion, in which multiple light-scattering effects will affect the measured absorbance and fluorescence spectra. To address this challenging problem, on the basis of the theory of photon diffusion approximation we derive the analytical models for absorbance and fluorescence spectra from tissue.

Diffuse reflectance

Because the basic measured quantities in our experimental setup are the diffuse reflectances at the excitation and emission wavelengths, our first task is to derive a model that can establish the relation between the reflectance and the absorbance of the fluorophore in the presence of scattering. For simplicity, we assume that the tissue is a homogeneous medium with a semi-infinite geometry. Then, the light propagation in the tissue can be described by the diffusion approximation, i.e., given by the diffusion equation (Ishimaru, 1978; Patterson et al., 1989; Yodh and Chance, 1995):

$$-D\nabla^2\psi(\boldsymbol{r}) + \mu_a\psi(\boldsymbol{r}) = S(\boldsymbol{r}) \tag{1}$$

where $\psi(\boldsymbol{r})$ represents the photon fluence rate at position $\boldsymbol{r} = (\rho, z)$, where ρ is the radial distance from the incident beam and z is the depth within tissue. $S(\boldsymbol{r})$ is the photon source in the tissue; $D \approx [3\mu_s']^{-1}$ is the diffusion coefficient for a turbid medium, such as biological tissue (Patterson et al., 1989); and μ_a, μ_s' are the optical absorption coefficient and the reduced scattering coefficient of tissue, respectively.

As has been described elsewhere (Patterson et al., 1989; Farrell et al., 1992), a Green function can be used to approximate $\psi(\boldsymbol{r})$ produced by a point source incident at $(0, z_0)$ for an infinite tissue boundary. The solution to a semi-infinite boundary condition, a good analog to our experimental illumination, is deduced by adding a negative or image source to the infinite case (Eason et al., 1987; Patterson et al., 1989):

$$\psi(\rho, z) = \frac{1}{4\pi D}\left(\frac{e^{-\mu_{eff}r_1}}{r_1} - \frac{e^{-\mu_{eff}r_2}}{r_2}\right) \tag{2}$$

where $r_1 = [(z - z_0)^2 + \rho^2]^{1/2}$ and $r_2 = [(z + z_0)^2 + \rho^2]^{1/2}$; $\mu_{eff} = [3\mu_a(\mu_a + \mu_s')]^{1/2}$ is defined as the effective attenuation coefficient, and $\delta_{eff} = 1/\mu_{eff}$ represents the effective penetration depth that characterizes the penetration of diffuse light into the tissue.

From Eq. 2, the measured diffuse reflectance from the tissue surface at $(\rho, 0)$ can be given by calculating the photon current leaving the tissue at $z = 0$

$$R(\rho) = -D\nabla\psi|_{z=0} = \frac{z_0}{2\pi}\left(\mu_{eff} + \frac{1}{\sqrt{z_0^2 + \rho^2}}\right)\frac{e^{-\mu_{eff}\sqrt{z_0^2+\rho^2}}}{z_0^2 + \rho^2} \tag{3}$$

where the parameter z_0 represents the diffusion range, i.e., the depth at which scattering events are assumed to produce an isotropic point source. It equals the reduced mean free path $mfp' = 1/(\mu_a + \mu_s')$ traveled by photons in tissue. For a pencil beam (e.g., focused beam) of strength S_0 incident normal to the tissue surface, the source distribution inside the tissue is $S_0\delta[z_0 - 1/(\mu_a + \mu_s')]$ (Eason et al., 1987). Hence, the total diffuse reflectance from the tissue can be calculated by integrating Eq. 3 for the whole source distribution and along the surface,

$$\begin{aligned} R &= \int_0^\infty\int_0^\infty R(\rho)S_0\delta\left[z_0 - \frac{1}{(\mu_a + \mu_s')}\right]dz_0 2\pi\rho d\rho \\ &= S_0\frac{\mu_s'}{\mu_a + \mu_s'}\frac{1}{1 + \sqrt{3\left(1 - \frac{\mu_s'}{\mu_a + \mu_s'}\right)}} \end{aligned} \tag{4}$$

This is the basic analytical expression that will be used below to derive the absorbance caused by the presence of fluorescent dye in the perfused mouse heart.

Absorbance induced by the fluorescent dye in tissue

If we assume that the fluorophore is distributed homogeneously within the tissue, the concentration of fluorophore can be derived from the measured diffuse reflectances before and after fluorophore injection. It is quite usual and convenient to present the results in terms of absorbance A^λ, which is given by

$$A^\lambda = \log_{10}\frac{R_0^\lambda}{R^\lambda} \tag{5}$$

where R_0^λ and R^λ are obtained pre- and post-loading of fluorescence. In our experiments, the additional optical absorption due to the fluorophore presence in the tissue is much less than that of tissue itself; the resultant change in the detected reflectance is so small that it can be expressed

as (Patterson et al., 1989)

$$A^{\lambda} = -0.434\mu_{af}^{\lambda}\frac{d}{d\mu_a}\log_e R^{\lambda} \quad (6)$$

where $\mu_{af}^{\lambda} = C\varepsilon^{\lambda}$ is the absorption coefficient of the fluorophore in tissue; C and ε^{λ} are the concentration and the extinction coefficient of fluorophore at the wavelength λ.

It should be pointed out that only the change of absorption induced by the presence of the fluorophore is considered in the derivation of Eq. 6. As a matter of fact, the reflected light is attributed to the photons propagating through and re-emitted from scattering tissue, the variation of tissue scattering induced by fluorophore presence could result in an additional error in the detected A^{λ}. This effect could be significant in the perfused beating heart because the perfusate is changed from one without to one with Rhod-2. For instance, Fig. 2 *A* shows the absorbance spectrum after loading Rhod-2 into the mouse heart. The absorbance was obtained according to Eq. 5, which compares the observed reflectance with that before Rhod-2 loading. As we expected, the infusion of Rhod-2 into the heart induces a significant increase in absorbance at 524 nm, because Rhod-2 absorbs light at this wavelength. However, a small increase in absorbance is also visible in the emission band longer than 580 nm, though Rhod-2 does not absorb light in this range. This is presumably due to the change in tissue scattering associated with the presence of Rhod-2 in the perfusate. As indicated in Fig. 2 *A*, this spurious change caused by the change of scattering in the tissue results in 25% overestimation of the Rhod-2 absorbance in the Rhod-2 absorption band (e.g., at 524 nm). It may vary with time and from subject to subject, and so must be accounted for.

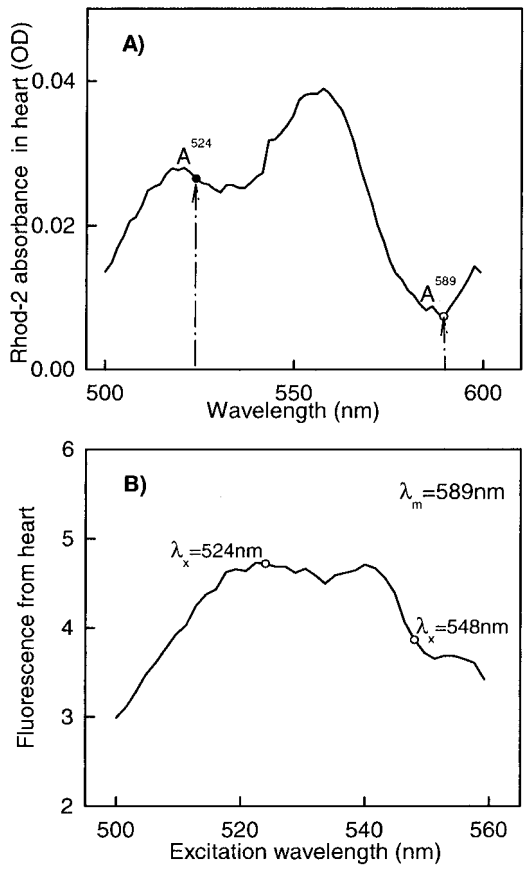

FIGURE 2 Reflected absorbance (*A*) and excitation spectrum (*B*) of Rhod-2 from the perfused mouse heart. *A* was obtained according to Eq. 5; *B* was obtained from the excitation spectral ratio between post- and pre-loading of Rhod-2.

If the artifacts due to changes in tissue scattering during perfusion are further taken into account, Eq. 6 can be rewritten as

$$\begin{aligned} A^{\lambda} &= \Delta\mu_a^{\lambda}\frac{\partial\log_{10}R^{\lambda}}{\partial\mu_a} + \Delta\mu_s'^{\lambda}\frac{\partial\log_{10}R^{\lambda}}{\partial\mu_s'} \\ &= -\mu_{af}^{\lambda}\xi_a^{\lambda} + \Delta\mu_s'^{\lambda}\zeta_{s'}^{\lambda} \end{aligned} \quad (7)$$

The first term on the right-hand side of the equation denotes the contribution of the absorption change to the detected absorbance A^{λ} when tissue scattering is unchanged (i.e., μ_s' is constant). The second term denotes the influence of the change in tissue scattering when μ_a is constant. It is quite clear that Eq. 6 is an approximation of Eq. 7 under the assumption that the variation induced by tissue scattering is negligibly small.

The coefficients ξ_a^{λ} and ζ_s^{λ} in Eq. 7 can be derived by differentiating Eq. 4 in logarithmic scale with respect to μ_a and μ_s' to give,

$$\begin{aligned} \xi_a^{\lambda} &= \left.\frac{\partial\log_{10}R^{\lambda}}{\partial\mu_a}\right|_{\mu_s'} = -0.434[3D + \tfrac{3}{2}\delta_{eff}R^{\lambda}] \\ \zeta_{s'}^{\lambda} &= \left.\frac{\partial\log_{10}R^{\lambda}}{\partial\mu_s'}\right|_{\mu_a} = 0.434[3D + \tfrac{3}{2}\delta_{eff}R^{\lambda}] \end{aligned} \quad (8)$$

Substituting Eq. 8 into Eq. 7 yields,

$$\begin{aligned} A^{\lambda} = 0.434\{&[\mu_{af}^{\lambda}[3D + \tfrac{3}{2}\delta_{eff}R^{\lambda}]] \\ &+[\Delta\mu_{s'}^{\lambda}[3D + \tfrac{3}{2}\delta_{eff}R^{\lambda}]]\} \end{aligned} \quad (9)$$

The equation relates the absorbance to the variations of absorption and scattering of tissue due to the infusion of fluorophore. It can be seen that the measured absorbance will be modified by the scattering changes due to fluorophore infusion and needs to be corrected. To remove the second bracket on the right-hand side in Eq. 9, we use a relative, two-wavelength absorbance method pioneered by Chance (1951). If the reflected intensities at the wavelengths of λ_1 and λ_2 are detected, the relative absorbance

difference between these wavelengths is:

$$A^{\lambda_1,\lambda_2} = \log_{10}\frac{R^{\lambda_1}}{R^{\lambda_2}} \tag{10}$$

and can be rewritten as,

$$A^{\lambda 1,\lambda 2} = [\Delta\mu_a^{\lambda_1}\xi_a^{\lambda_1} - \Delta\mu_a^{\lambda_2}\xi_a^{\lambda_2}] + [\Delta\mu_s'^{\lambda_1}\zeta_{s'}^{\lambda_1} - \Delta\mu_s'^{\lambda_2}\zeta_{s'}^{\lambda_2}] \tag{11}$$

if a similar mathematical derivation is applied as used to get Eq. 9. This equation can be further simplified for the case in which the scattering properties of tissue are approximately identical at λ_1 and λ_2 before adding fluorescent dye. Two such wavelengths can be found because in the visible and NIR range, μ_s' is a slow-varying function of wavelength (Cheong et al., 1990). For $\lambda_1 - \lambda_2 < 100$ nm in our experiment, it can be assumed that $\Delta\mu_s'^{\lambda 1} = \Delta\mu_s'^{\lambda 2}$, $D^{\lambda 1} = D^{\lambda 2}$, and $\delta_{eff}^{\lambda 1} = \delta_{eff}^{\lambda 2}$. By choosing λ_2 such that the fluorophore does not absorb, i.e., $\Delta\mu_a^{\lambda 2} = 0$; then Eq. 11 can be rewritten as:

$$\begin{aligned} A^{\lambda 1,\lambda 2} &= \Delta\mu_a^{\lambda 1}\xi_a^{\lambda 1} + \Delta\mu_s'[\zeta_{s'}^{\lambda 1} - \zeta_{s'}^{\lambda 2}] \\ &= 0.434\{\mu_{af}^{\lambda 1}[3D + \tfrac{3}{2}\delta_{eff}R^{\lambda 1}] \\ &\quad + \Delta\mu_s'[\tfrac{3}{2}\delta_{eff}(R^{\lambda 1} - R^{\lambda 2})]\} \end{aligned} \tag{12}$$

This equation reveals that an appropriate selection of the wavelengths λ_1 and λ_2 so that the reflected intensities at these wavelengths are close (i.e., $R^{\lambda 1} \approx R^{\lambda 2}$) can eliminate the influence of tissue scattering changes as represented by the second term in Eq. 12. This leads to the simplified relation:

$$A^{\lambda 1,\lambda 2} = \log_{10}\frac{R^{\lambda 1}}{R^{\lambda 2}} = 0.434\,\mu_{af}^{\lambda_1}[3D + \tfrac{3}{2}\delta_{eff}R^{\lambda 1}] \tag{13}$$

Equation 13 provides a useful model to analyze the relation of the absorbance in the excitation band with the optical properties of tissue and fluorophore in highly scattering tissue.

Fluorescence emission from tissue

In principle, the diffusion theory can also be used to describe the propagation of fluorescence light in a scattering tissue if a proper model is used to simulate the fluorescence source for Eq. 1.

In scattering tissue, the source term for the fluorescence emission $S^{\lambda m}(\boldsymbol{r}')$ at position $\boldsymbol{r}'$ is proportional to the excitation light absorbed by the fluorophores at $\boldsymbol{r}'$ (i.e., $\mu_{af}^{\lambda x}N_x(\boldsymbol{r}')$) and the quantum efficiency $\Phi^{\lambda x,\lambda m}$ of fluorescence, which is excited at λ_x and emitted at λ_m. To obtain the fluorescence that reaches the surface at position $\boldsymbol{r}$, i.e., $F^{\lambda x,\lambda m}(\boldsymbol{r})$, one must calculate the fluorescence photon density $N_f(\boldsymbol{r})$ or the fluence rate $\psi_f(\boldsymbol{r}) = cN_f(\boldsymbol{r})$ (c is the speed of light in tissue). This can be derived by spatially convolving $S^{\lambda m}(\boldsymbol{r}')$ with the escape function $E^{\lambda m}(\boldsymbol{r}' - \boldsymbol{r})$ of the fluorescence light,

$$N_f(\boldsymbol{r}) = \mu_{af}^{\lambda x}\Phi^{\lambda x,\lambda m}\int_{r'} N^{\lambda x}(\boldsymbol{r}') \times E^{\lambda m}(\boldsymbol{r} - \boldsymbol{r}')d\boldsymbol{r}' \tag{14}$$

where $r' = (\rho^2 + z^2)^{1/2}$ varies with the variables ρ in the horizontal direction and z in the vertical direction. Thus, this convolution is actually a two-dimensional integral and is analytically unsolvable without appropriate approximations. To tackle this problem and obtain an analytical solution to Eq. 14, one approach is to simplify the convolution to one dimension only in the z direction, assuming that both $N^{\lambda x}$ and $E^{\lambda m}$ decrease exponentially as a function of z either with empirical attenuation coefficients or within diffusion approximations (van der Putten and van Gemert, 1983; Potter and Mang, 1984; Gmitro et al., 1988; Richards-Kortum et al., 1989). The alternative is to use the photon migration method to derive the relationship of photon densities (i.e., fluences) between the fluorescence excitation and emission, thus circumventing the complexity of the convolution calculation (Wu et al., 1993; Patterson and Pogue, 1994). As has been described elsewhere (Patterson and Pogue, 1994), in the case of a continuous-wave excitation, the fluorescence photon density $N_f(\boldsymbol{r})$ can be given by

$$N_f(\boldsymbol{r}) = \frac{\mu_{af}^{\lambda x}\Phi^{\lambda x,\lambda m}}{\mu_a^{\lambda x} - \mu_a^{\lambda m}}[N^{\lambda m}(\boldsymbol{r}) - N^{\lambda x}(\boldsymbol{r})] \tag{15}$$

where $N^{\lambda m}(\boldsymbol{r})$ is the excitation photon density that would be observed if the excitation wavelength were changed to λ_m. The fluorescence emission from the tissue surface at $(0, \rho)$ can be derived as a summation of all the photon currents leaving the tissue from there,

$$\begin{aligned} F^{\lambda x,\lambda m}(\boldsymbol{r})|_{z=0} &= -D\nabla[cN_f(\boldsymbol{r})]|_{z=0} \\ &= \frac{\mu_{af}^{\lambda x}\Phi^{\lambda x,\lambda m}}{\mu_a^{\lambda x} - \mu_a^{\lambda m}}[R^{\lambda m}(\rho) - R^{\lambda x}(\rho)] \end{aligned} \tag{16}$$

The total fluorescence emission over the entire tissue surface can be acquired by a spatial integration over the entire surface as a summation of all lateral positions ρ

$$F^{\lambda x,\lambda m} = \frac{\mu_{af}^{\lambda x}\Phi^{\lambda x,\lambda m}}{\mu_a^{\lambda x} - \mu_a^{\lambda m}}[R^{\lambda m} - R^{\lambda x}] \tag{17}$$

where $\mu_a^{\lambda x} = \mu^{\lambda x} + \mu_{af}^{\lambda x}$, $\mu_a^{\lambda m} = \mu^{\lambda m} + \mu_{af}^{\lambda m}$ are the total absorption coefficients at the excitation and emission wavelengths of λ_x and λ_m, respectively. $R^{\lambda x}$ and $R^{\lambda m}$ are the total reflectances at λ_x and λ_m in the presence of fluorophore in tissue.

EXTRACTING FLUORESCENCE QUANTUM YIELD FOR $[Ca^{2+}]_i$ DETERMINATION

The model analysis has been general so far, in the sense that neither the specific optical properties of the Ca^{2+} probe nor those of the heart tissue have been considered in the above derivation. In this section, however, the optimal selection of the wavelengths used for the absorbance and fluorescence detection by which the Ca^{2+} is measured by using Rhod-2 in perfused heart will be discussed. For this purpose, the ratiometric method evaluating the fluorescence-to-absorbance ratio is introduced to extract the quantum yield $\Phi^{\lambda x,\lambda m}$ of the Ca^{2+}-dependent fluorescence. As a consequence, this ratio, F/A, is independent of the probe concentration in the heart, thus making Rhod-2 a quantitative calcium indicator. More importantly, our theoretical modeling demonstrates that F/A can be used to determine the concentration of cytosolic calcium $[Ca^{2+}]_i$, and the distortion induced by the tissue optical properties and the detection geometry are eliminated.

Optimal selection of absorbance and fluorescence wavelengths

Although the Ca^{2+}-sensitive probe, Rhod-2, is excited and emitted in the visible range of 500–630 nm where tissue chromophores (mainly myoglobin in perfused heart) absorb much less light than in the UV range, the tissue optical properties (absorption and scattering) still play an important role in the excitation and fluorescence detection. This so-called "inner filter" effect, to a great extent, depends on tissue oxygenation. Fig. 2 *B* is the fluorescence excitation spectrum from a perfused heart. Unlike in calcium solution where Rhod-2 exhibits higher fluorescence emission excited at 548 nm because of a higher absorption at this wavelength, in heart tissue the excitation at 524 nm is more efficient than at 548 nm as a result of inner filtering by the tissue. Fig. 3 *A* shows the reflected-absorption spectra obtained from the surface of a perfused mouse heart with varying oxygenation state from normoxic to hypoxic. Fig. 3 *B* indicates the isosbestic wavelengths of 524, 548, 568, and 589 nm for the heart tissue, determined by comparing the normoxic and hypoxic spectra. Fig. 3 *C* shows the fluorescence spectra of Rhod-2 measured from the heart in both normoxia and hypoxia, respectively. It demonstrates that the fluorescence intensity of Rhod-2 changes with the oxygenation of the heart, except at the isosbestic wavelengths.

To minimize the influence of the tissue absorption changes caused by the oxygenation status of the heart on absorbance and fluorescence detection, two isosbestic wavelengths are needed for fluorescence excitation and fluorescence emission, respectively. However, the absorbances at these two wavelengths are required to be nearly equal to eliminate the influence of tissue scattering. In this study, $\lambda_x = 524$ nm and $\lambda_m = 589$ nm are chosen as

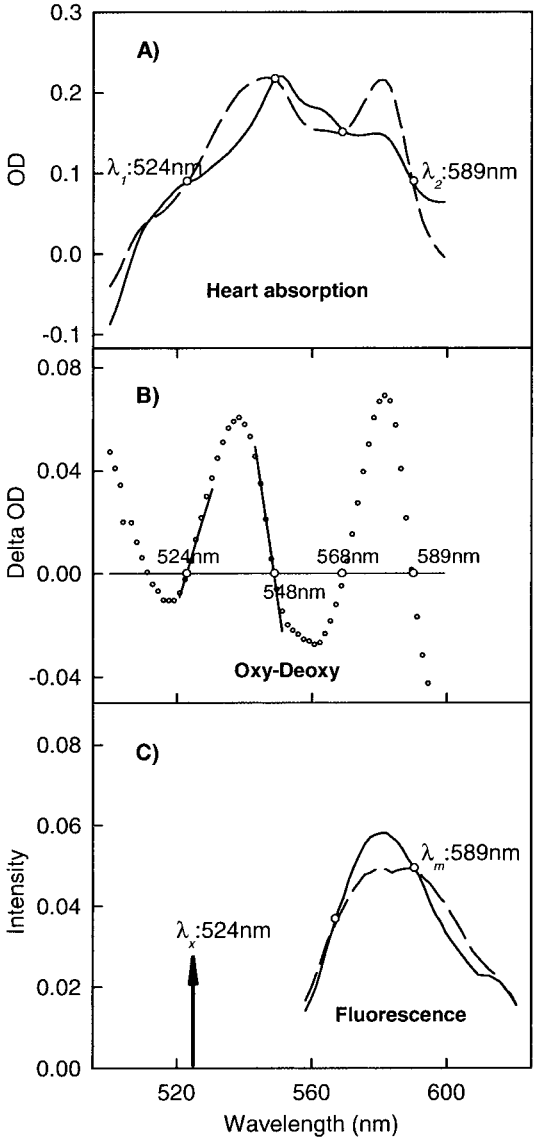

FIGURE 3 Fluorescence excitation, emission, and absorbance measurements are chosen at the isosbestic wavelengths (*circles*) of myoglobin to minimize the effects of tissue absorption change caused by oxygenation changes in the Rhod-2 loaded heart. (*A*) Reflected absorption spectra from oxygenated heart (*dashed line*) and deoxygenated heart (*solid line*). (*B*) Difference in absorption spectrum of a heart in oxygenated and deoxygenated state. (*C*) Fluorescence spectra obtained from oxygenated heart (*dashed line*) and deoxygenated heart (*solid line*).

excitation and emission wavelengths, respectively. These two wavelengths are also used as λ_1 and λ_2 for the determination of the differential absorbance $A^{\lambda 1,\lambda 2}$ by using Eq. 13. The rationales for and importance of selecting these two wavelengths are as follows:

1. Rhod-2 absorbs light at 524 nm and does not absorb at 589 nm, thus satisfying the requirement specified in Eq. 13, i.e., $\Delta\mu_a^{\lambda 1} \neq 0$, and $\Delta\mu_a^{\lambda 2} = 0$;
2. $\lambda_m - \lambda_x \leq 100$ nm, the difference of the tissue scattering properties at the excitation and emission wavelengths is

negligible (Cheong et al., 1990), the differences of D and $\Delta\mu_s'$ between these two wavelengths can be ignored;

3. The reflectance spectra of heart tissue at these two wavelengths are approximately equivalent; in other words, $R^{\lambda 1} \sim R^{\lambda 2}$, and the second term on the right-hand side of Eq. 12 representing the change in tissue scattering can be neglected. The influence of the fluctuation in tissue scattering on $A^{\lambda 1,\lambda 2}$ can thus be minimized;
4. At these two wavelengths, both scattering and absorption (excluding fluorophore) of heart tissue are approximately equal; therefore, the penetration depths should be approximately the same according to $\delta_{eff} = [3\mu_a(\mu_a + \mu_s')]^{-1/2}$;
5. Both 524 and 589 nm are isosbestic wavelengths; thus, the influence of tissue absorption change due to tissue oxygenation on the optical measurements is minimized. Furthermore, the change in absorbance at 524 nm with oxygenation is smaller than at 548 nm (see slope in Fig. 3 *B*).

Fluorescence-to-absorbance ratio

As discussed above, 524 and 589 nm are specified as excitation and emission wavelengths to measure the Ca^{2+}-dependent fluorescence in the perfused heart. The fluorescence emission given in Eq. 17 can be simplified as

$$\begin{aligned} F^{\lambda x,\lambda m} &= \Phi^{\lambda x,\lambda m}(-1)\mu_{af}^{\lambda x}\frac{\Delta R}{\Delta\mu_a} \\ &\approx \Phi^{\lambda x,\lambda m}(-1)\mu_{af}^{\lambda x}\frac{dR}{d\mu_a} \\ &= \mu_{af}^{\lambda x}\Phi^{\lambda x,\lambda m}\{R^{\lambda x}[3D + \tfrac{3}{2}\delta_{eff}R^{\lambda x}]\} \end{aligned} \quad (18)$$

It is almost impossible to collect the total emission over the entire tissue surface without utilizing an integrating sphere. However, to avoid the strong specular reflectance due to mismatch of reflective index at the interface between air, glass, and tissue, the detection optics is chosen to have a deflection angle of α_F off the normal direction of the incident beam. With a solid angle of Ω_F, the fluorescence intensity collected by the detection system is a portion of the total emission multiplied by a geometric factor $G(\Omega_F, \alpha_F)$ $(= \Omega_F/2\pi \cos \alpha_F)$ according to Lambert's law (Wilson and Jacques, 1990). Therefore, for the fluorescence detection geometry with a $G(\Omega_F, \alpha_F)$ used in our experiment, Eq. 18 becomes

$$\begin{aligned} F^{\lambda x,\lambda m} &= G(\Omega_F, \alpha_F)\mu_{af}^{\lambda x} \\ &\quad \cdot \Phi^{\lambda x,\lambda m}\{R^{\lambda x}[3D + \tfrac{3}{2}\delta_{eff}R^{\lambda x}]\} \end{aligned} \quad (19)$$

Combining Eqs. 13 and 19 and applying $\lambda_1 = \lambda_x$ and $\lambda_2 = \lambda_m$ yields

$$\frac{F}{A} = \frac{F^{\lambda x,\lambda m}}{A^{\lambda 1,\lambda 2}} = (0.434)^{-1}G(\Omega_F, \alpha_F)R^{\lambda x}\Phi^{\lambda x,\lambda m} \quad (20)$$

This equation indicates that the ratio F/A remains proportional to the quantum yield Φ, while the absorption coefficient $\mu_{af}^{\lambda x}$ is excluded by this ratio calculation. This implies that the influence of Rhod-2 concentration washout during perfusion can be eliminated by this ratiometric method. It must also be noted that the geometry factor G disappears in the expression of $A^{\lambda 1,\lambda 2}$. This is because the reflectances at these two wavelengths are measured with the same detection optics, and the geometric factors affecting the absolute signals at each wavelength can be eliminated by their ratio in terms of $A^{\lambda 1,\lambda 2}$ in Eq. 10.

$[Ca^{2+}]_i$ determination

The ratio F/A can be used to calculate cytosolic calcium concentration $[Ca^{2+}]_i$ by the following equation:

$$[Ca^{2+}]_i = K_d \frac{\dfrac{F_t^{\lambda x,\lambda m}}{A_t^{\lambda 1,\lambda 2}}}{\dfrac{F_{max}^{\lambda x,\lambda m}}{A_{max}^{\lambda 1,\lambda 2}} - \dfrac{F_t^{\lambda x,\lambda m}}{A_t^{\lambda 1,\lambda 2}}} \quad (21)$$

where $K_d = 710$ nM is the dissociation coefficient for Rhod-2 and calcium calibrated in vitro (Del Nido et al., 1998). F_t and A_t denote the Ca^{2+}-dependent fluorescence and differential absorbance at the excitation and the emission wavelengths at time t. F_{max} is the maximal fluorescence calibrated in situ by tetanizing the heart at high perfusate calcium in the presence of a sarcoplasmic reticulum ATPase inhibitor, and A_{max} is the absorbance during tetanization. Equation 21 assumes that $F^{\lambda x,\lambda m}$ is zero at $[Ca^{2+}]_i = 0$ due to a ~100-fold change in the fluorescence with calcium binding of Rhod-2 (Haugland, 1996). Therefore, the minimal fluorescence is assumed to be equal to the background fluorescence (Del Nido et al., 1998). F_t and F_{max} can be obtained by subtracting the background fluorescence before Rhod-2 loading from the fluorescence intensities.

It should be pointed out that, although the ratio F/A is affected by the factors $R^{\lambda x}$ and G as indicated in Eq. 20, the influence of these factors can be eliminated in Eq. 21 for $[Ca^{2+}]_i$ determination provided that they are unchanged or measured during the experiment and during determination of the maximal fluorescence calibration.

MATERIALS AND METHODS

Experiments were performed to verify the predictions of Eq. 20 and to validate Eq. 21 for the quantification of cytosolic calcium in the perfused mouse heart. In this section we describe the perfused mouse heart preparation and the experimental apparatus and procedures, with emphasis on the detection of the reflected absorbance and fluorescence from the perfused heart. To assess motion-induced artifacts of the beating heart and to ensure heart oxygenation, a noninvasive technique was introduced in our

experiment to monitor NADH and the absorption spectrum of the heart before Rhod-2 loading.

Mouse heart perfusion

The isolated mouse heart was perfused using the Langendorff method in a water-jacketed chamber at 37°C, and stimulated at 8 Hz. A balloon was inserted into the left ventricular cavity to monitor developed pressure simultaneously with the Rhod-2-labeled calcium transient. To suppress motion-induced artifacts and minimize the effects from the curvature of the epicardium, the mouse heart was gently placed against the optical window inside the chamber by immobilizing the perfusion cannula above the heart.

Apparatus

Optical experiments were performed using an SLM spectrofluorometer (Aminco SLM 8000, SLM Co., Springfield, IL). The light source used was an arc lamp connected to a computer-controlled monochromator to select the excitation wavelength within the region of 300–800 nm. After passing through a beam-splitter that reflects ~4% of the incident light for reference detection, the transmitted light was delivered onto the heart surface with a 2 mm beam spot. The fluorescence emission was collected with a biconvex lens ($f = 50$ mm) placed at 90° off the excitation beam, filtered by a second monochromator, and then detected by a cooled photomultiplier tube (PMT-F). To avoid the specular reflection from the air-glass-tissue interfaces, the perfusion chamber was positioned at 30° off the excitation beam. A long-pass filter (LPF) with a cutoff wavelength at 540 nm was inserted in front of the emission monochromator to block the scattered excitation photons, including the stray light from the slightly curved heart surface. The reflected diffuse light from the heart tissue was collected by a focal lens ($f = 30$ mm), mounted at 45° off the normal direction of the window plane to avoid the specular reflection. It was then delivered to another photomultiplier tube (PMT-A) through a flexible liquid light guide (Oriel Co. 77568, Stratford, CT). To eliminate the errors induced by the source intensity fluctuation, the fluorescence and reflectance signals were instantaneously compared to the reference signal by a reference PMT. These signals are acquired and stored in a computer via an A/D converter.

Compensation of motion- and oxygenation-induced artifacts

The motion of a beating heart can introduce a motion artifact affecting the measured Ca^{2+} fluorescence transient signal. Previous studies proposed improved chamber designs (Salama et al., 1987; Efimov et al., 1996) and an internal fluorescence standard to minimize this artifact and avoid ischemia (Koretsky et al., 1987). These methods required either complicated chamber design and precise pressure control or additional fluorescent dye infusion. In this study a simple and direct method is proposed, allowing utilization of a conventional water-jacketed bath (FP-295, Spectronic Instrument, Urbana, IL). As will be discussed later, this technique is based on our observation that the NADH emission at 465 nm exhibited a waveform whose amplitude is proportional to the heart's contractile motion. Therefore, the NADH signal acquired over several cardiac cycles permitted optimal adjustment of heart position and tension to minimize motion artifacts. Because the heart was gently placed against the window by fixing the perfusion cannula, this method has proven effective in maintaining normal physiological function in the perfused heart.

To monitor the oxygenation state of the heart, the reflected absorbance spectrum between 500 and 600 nm was measured together with the ratio of NADH fluorescence at 465 nm (excited at 365 nm) to the autofluorescence at 589 nm (excited at 524 nm). As discussed later, these parameters can be used to determine if the oxygenation state of the heart is adequate at the beginning of the experiment.

Fluorescence and absorbance measurements

During the experiment, 100 μg Rhod-2 (Molecular Probes, R-1243, Eugene, OR) was dissolved in 4 μl dimethylsulfoxide (DMSO) and 200 μl water, then mixed with 9 ml oxygenated Krebs solution and bolused through the perfusate. The Rhod-2 was added to a parallel perfusion line connected to the same reservoir. During bolusing the bolus line was opened and the other line was closed. This method resulted in no change in the important coronary flow rate, which averages at 1.9 ± 0.4 ml/min. Thus, the bolus concentration of Rhod-2 was 11 μg/ml and was infused for 4–5 min. The precise time depended on the coronary flow for an individual heart. Loading of Rhod-2 resulted in a 6.2 ± 1.9-fold increase ($n = 24$) in fluorescence over background fluorescence at the end of the 20–25 min washout period. Subsequently, Ca^{2+}-dependent fluorescence transients along with the corresponding left ventricular pressure signals were acquired at a sampling rate of 15 ms per point to provide ~8 points per cardiac cycle (stimulation rate = 8 Hz). At each data point, signal averaging was performed to reduce noise. To normalize the change of fluorescence signal due to Rhod-2 washout through the perfusate, the reflected absorbance spectrum was scanned from 500 to 600 nm in <15 s and the absorbance ratio between 524 nm and 589 nm was determined using Eq. 10. After five fluorescence and absorbance measurements were taken, the maximal calcium-dependent fluorescence signal was calibrated in situ using a high concentration of calcium perfusate (20 mM calcium chloride) with the sarcoplasmic reticulum Ca^{2+}-ATPase inhibitor, cyclopiazonic acid (10 μM, Sigma Chemical Co., St. Louis, MO) to tetanize the heart and saturate Rhod-2 with calcium ($n = 20$). Simultaneously, the diffuse reflectance was recorded to correct the effects due to scattering changes in the heart tissue. $[Ca^{2+}]_i$ was calculated using Eq. 21, in which F_t and F_{max} are the fluorescence intensities after subtracting the background autofluorescence before Rhod-2 loading.

The cyclopiazonic acid tetanization method was compared to the digitonin tetanization method, as used by Del Nido et al. (1998). In $n = 4$ experiments, digitonin (10 μm) was mixed with 9 ml perfusate and loaded through the coronary circulation into the heart.

To examine whether the changes in tissue scattering due to perfusate changes are wavelength-independent, graded concentrations of manganese chloride ($MnCl_2$, 25–1000 μm, $n = 12$) were infused into the heart after Rhod-2 loading. The absorbance spectrum within the wavelength of 500–600 nm was recorded after each administration.

RESULTS

Motion suppression and oxygenation state of the heart

Fig. 4 is a representative experiment showing the use of NADH fluorescence for suppression of motion-induced artifacts. Fig. 4 *A* shows that the background fluorescence at 589 nm, B_b^{589}, is too low to be useful to monitor motion-induced artifact before Rhod-2 loading. However, it can be seen in Fig. 4 *B* that the NADH emission, B_{NADH}^{465}, varies with heart contractile motion (180 phase delay), and was significantly reduced in amplitude when the heart was appropriately immobilized against the optical window (see Fig. 4 *B*, *right*) with improvement in the fluorescence transient signal as illustrated in Fig. 4 *C*. This suggests that B_{NADH}^{465} provides a simple and immediate estimation of the motion-induced noise. In 16 hearts motion-induced artifact, as determined by variation in NADH autofluorescence, was 4.6 ± 1.2% from immobilized hearts. This was calculated by using $\Delta B_{NADH}^{465}/B_{NADH}^{465}$, where ΔB_{NADH}^{465} is the NADH

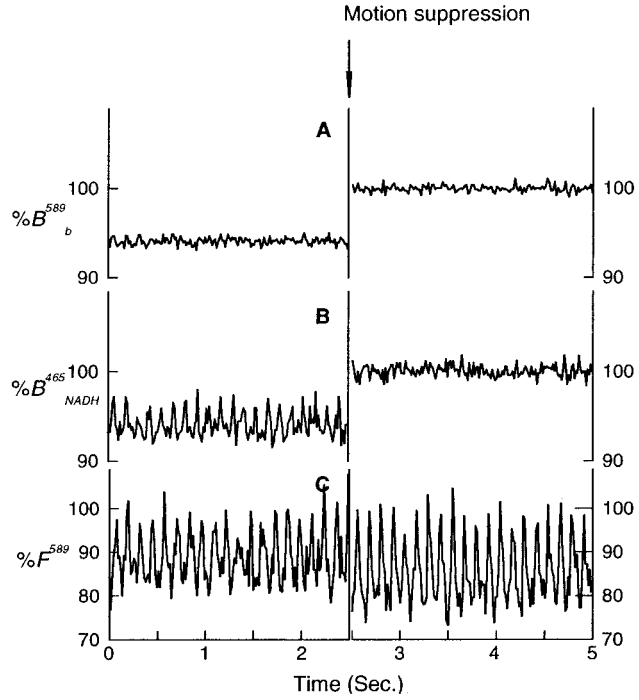

FIGURE 4 Identification of motion artifacts by monitoring NADH autofluorescence before Rhod-2 loading, allowing optimization of motion suppression by positioning of the heart. Background fluorescence emission at 589 nm (*A*) excited at 524 nm, autofluorescence of NADH at 465 nm (*B*) excited at 365 nm obtained from the heart before loading Rhod-2, and the comparison of Ca^{2+}-dependent fluorescence transient signal before and after motion suppression (*C*). Note that these data have been normalized to their maximum values for comparisons before and after positioning the heart.

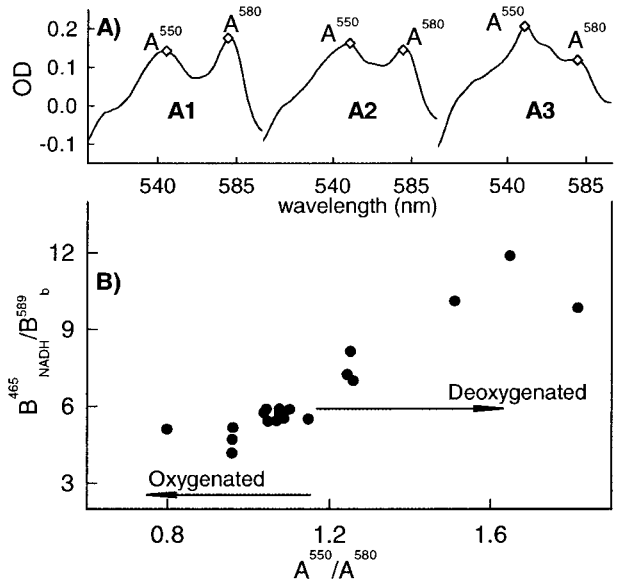

FIGURE 5 Monitoring of myocardial oxygenation of the perfused mouse hearts before loading Rhod-2. (*A*) Effects of the oxygenation state of myoglobin on the reflected absorption peaks of 550 and 580 nm. The oxygenation state was seen to vary with coronary flow. Occasionally, when perfusing hearts poor oxygenation is seen related to low coronary flow (A1 = 1.9 ± 0.4 ml/min, A2 = 1.3 ± 0.25 ml/min, and A3 = 1.1 ± 0.26 ml/min). Thus, in hearts with higher coronary flows a lower ratio of A^{550}/A^{580} is seen. (*B*) Relationship of the measured fluorescence ratio $B^{465}_{NADH}/B^{589}_{b}$ and absorbance ratio A^{550}/A^{580}.

variation amplitude and B^{465}_{NADH} is the normalized mean NADH autofluorescence intensity.

Fig. 5 *A* shows that myoglobin oxygenation markedly affects the ratio A^{550}/A^{580}, where A^{550} is the absorption peak at 550 nm (deoxy-sensitive) and A^{580} is that at 580 nm (oxy-sensitive). These data were obtained from a group of hearts, some of which inadvertently had low coronary flows. When perfusing mouse hearts we have noticed that occasionally hearts are dysfunctional related to low coronary flows that reduce oxygen delivery to the heart. Thus, this spectral ratio A^{550}/A^{580} permits real-time monitoring of the oxygenation of the mouse heart tissue during the experiment. Also, B^{465}_{NADH} varies with the oxygenation state, whereas B^{589}_{b} measured at the isosbestic point of 589 nm is oxy-insensitive, so that $B^{465}_{NADH}/B^{589}_{b}$ provides another measure of monitoring the oxygenation state of the heart. The relationship between $B^{465}_{NADH}/B^{589}_{b}$ and A^{550}/A^{580} obtained from 20 hearts is illustrated in Fig. 5 *B*. Mouse hearts were considered well-oxygenated if $B^{465}_{NADH}/B^{589}_{b} \leq 6$ or $A^{550}/A^{580} \leq 1$. Thus, we now use the absorbance spectra at the beginning of the experiment to determine whether a heart is well-oxygenated.

Rhod-2 washout and fluorescence-absorbance normalization

Fig. 6 *A*, *left* shows the calibrated absorbance spectra during the washout period, e.g., 25 min after Rhod-2 was loaded, which were obtained by using Eq. 10 with $\lambda_2 = 589$ nm. Fig. 6 *A*, *right* shows the corresponding fluorescence spectra of Rhod-2 from the same heart. Both figures clearly indicate that Rhod-2 gradually leaks out of the heart tissue, resulting in a decrease in $A^{524,589}$ and $F^{524,589}$.

In Fig. 6 *B* the closed circles show the decay of the absorbance $A^{524,589}$ during the washout period, whereas the open circles show the decay of the mean fluorescence $F^{524,589}$. It can be seen that $A^{524,589}$ decreases in proportion with $F^{524,589}$ during dye washout; in other words, with Rhod-2 concentration. This result confirms our theoretical predictions in Eqs. 13 and 19. Fig. 6 *C* shows the ratios of F/A with excitation at 524 or 548 nm. As illustrated by the squares in Fig. 6 *C*, $F^{524,589}/A^{524,589}$ is independent of the washout time or Rhod-2 concentration, thus confirming the feasibility of the ratiometric technique, i.e., Eq. 20, which we propose to effectively eliminate the influence of dye concentration changes induced by heart perfusion on the $[Ca^{2+}]_i$ determination. To determine which isosbestic wavelength is optimal, we also plot the ratio of $F^{548,589}/A^{548,589}$ as a function of time in Fig. 6 *C*. In $n = 3$ experiments, the mean change in $F^{548,589}/A^{548,589}$ was 15.1 ± 5.3% over 20

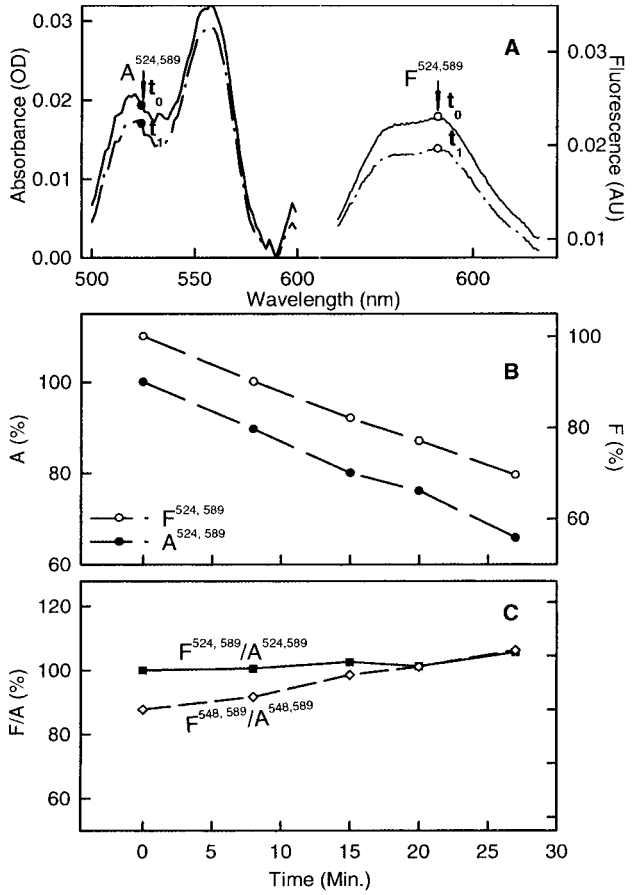

FIGURE 6 An example of the effects of Rhod-2 washout from the heart on absorbance and fluorescence signals. (*A*, *left*): Absorbance spectra of Rhod-2 at time t_0 and t_1, calibrated at $\lambda_2 = 589$ nm using Eq. 10; (*A*, *right*): Ca^{2+}-dependent fluorescence spectra of Rhod-2 at the same time when excited at 524 nm, in which the background fluorescence is subtracted. (*B*) Changes of Ca^{2+}-dependent mean fluorescence $F^{524,589}$ (*open circle*, obtained by time-averaging transients), and absorbance $A^{524,589}$ (*closed circle*) as a function of time. (*C*) Fluorescence emissions at 589 nm when excited at 524 nm (*solid squares*), or at 548 nm (*open diamond*) normalized by the corresponding absorbances, indicating the independence of $F^{524,589}/A^{524,589}$ on Rhod-2 washout.

min with dye washout, whereas with $F^{524,589}/A^{524,589}$ this was only 2.0 ± 1.5%, indicating that $F^{548,589}/A^{548,589}$ was dependent on dye concentration, unlike $F^{524,589}/A^{524,589}$.

Tissue scattering change during Mn^{2+} infusion and corrected F_{max}

Equation 13 is validated under the assumption that the change of tissue scattering-properties due to perfusate changes are approximately identical at wavelengths of λ_1 and λ_2. To investigate this hypothesis, we measured the changes of reflectance spectra while adding various doses of manganese. Fig. 7 shows an example illustrating that the overall spectral absorption within 500–600 nm decreases in a wavelength-independent manner with $[Mn^{2+}]$. As we

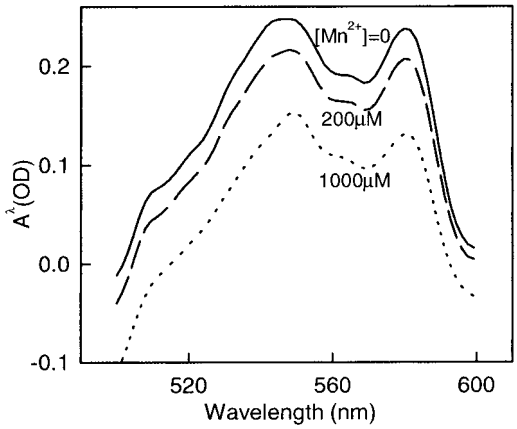

FIGURE 7 Reflected absorption spectra obtained from the mouse heart with Mn^{2+} infusion from $[Mn^{2+}] = 0$ (*solid line*), 200 (*dashed line*), to 1000 μM (*dotted line*).

found that increasing $[Mn^{2+}]$ did not modulate the absorption spectrum of Rhod-2, this decrease must have resulted from a change of pathlength L within the narrow band of 500–600 nm due to Mn^{2+} perfusion, which was dose-dependent. We believe that adding Mn^{2+} introduces a slight osmotic pressure gradient between the intra and extracellular fluid and causes cellular volume changes, thus resulting in an increase in tissue scattering. Similar observations have been reported with liver perfusion (Chance et al., 1995). This previous study proposed a linear relation between ΔL and $\Delta\mu_s'$ (Liu et al., 1996); therefore, it is a reasonable assumption that the change of tissue scattering is wavelength-independent, i.e., $\Delta\mu_s'^{\lambda 1} \approx \Delta\mu_s'^{\lambda 2}$ within the 500–600 nm range.

Similar changes in tissue-scattering properties have been found at the three isosbestic wavelengths of 524, 548, and 589 nm during heart tetanization, and Fig. 8 *B* shows typical time-dependent reflectance R^{524} and fluorescence $F_{max}^{524,589}$ traces. At the isosbestic point of 524 nm, the increase of R^{524} must be caused by tissue scattering rather than endogenous absorption due to any oxygenation changes or myoglobin leaking out of cells because the absorbance spectra before and after tetanization overlap at the isosbestic points, as shown in Fig. 8 *A*. This change in tissue scattering is likely due to hypoxia and contraction during tetanization, resulting in changes in tissue properties such as cell size or refractive index differences between intra and extracellular fluid. This increase in tissue scattering results in an increase in R^{524} and $F_{max}^{524,589}$, in addition to that resulting from an increase in Φ due to increased Ca^{2+} (see Eq. 19).

The influence of this increase in R^{524} on $F_{max}^{524,589}$ can be corrected effectively by multiplying $F_{max}^{524,589}$ with the ratio of R^{524} pre- to post-tetanization. The corrected $F_{max}^{524,589}$ over $A_{max}^{524,589}$ results in a steady-state maximal value as shown in Fig. 8 *B*, which is used in Eq. 21 for the $[Ca^{2+}]_i$ determination.

For comparison, Fig. 9 shows heart tetanization with digitonin. As we can see from Fig. 9 *B* the fluorescence

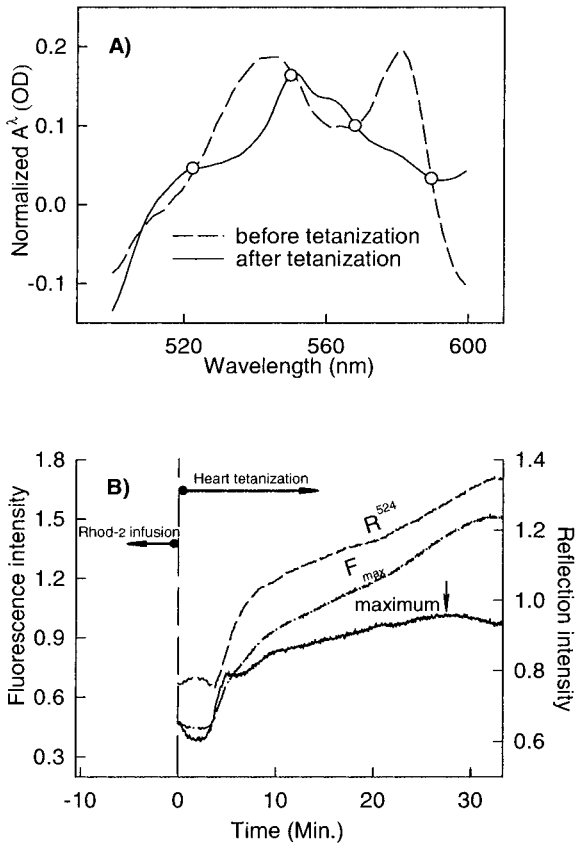

FIGURE 8 (*A*) Comparison of absorbance spectra before and after tetanization with cyclopiazonic acid, normalized at 589 nm. Open circles indicate the isosbestic wavelengths of myoglobin. (*B*) Changes of fluorescence $F^{524,589}$ (*dotted line*) and reflectance R^{524} (*dashed line*) due to changes in tissue scattering during heart tetanization. The corrected $F^{524,589}$ over $A^{524,589}$ results in a steady maximum (*solid line*), thus eliminating the influence of tissue scattering changes on the $[Ca^{2+}]_i$ calculation using Eq. 21.

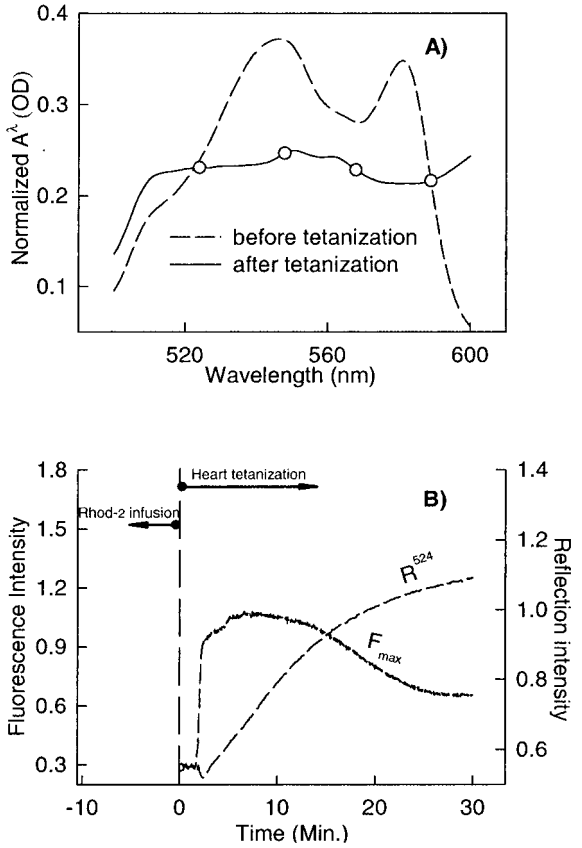

FIGURE 9 (*A*) Absorbance spectra before and after heart tetanization using digitonin, normalized at 589 nm. Open circles indicate the isosbestic wavelengths of myoglobin. (*B*) Changes of fluorescence $F^{524,589}$ (*dotted line*) and reflectance R^{524} (*dashed line*) during heart tetanization.

reaches a maximal value in ~5 min after tetanization (F_{max} uncorrected = 282 ± 63%) and then decreases significantly along with an increase in R^{524}, so that at ~25 min fluorescence falls to 169 ± 53%. Interestingly, the absorbance spectrum after digitonin tetanization is very much flattened in the myoglobin absorption range of 500–600 nm, as shown in Fig. 9 *A*. Thus, the fluorescence decrease is likely caused by wash out of cellular contents related to digitonin permeabilization of surface membranes. For this reason, we have preferred to tetanize the heart with cyclopiazonic acid rather than digitonin, though there is no significant difference in the maximal fluorescence increase between the two methods. The uncorrected F_{max} with cyclopiazonic acid is 294 ± 59%, and with digitonin is 282 ± 63% (p = ns) relative to the pre-tetanization mean fluorescence value. Of note, because of the leakage phenomenon with digitonin we cannot correct F_{max} for the digitonin method. The corrected F_{max} for cyclopiazonic acid method is 223 ± 40%, and it is this value which is used in the calculation of intracellular calcium concentration.

Ca^{2+}-transients in perfused mouse heart

Fig. 10 shows the normalized Ca^{2+}-dependent fluorescence transient labeled with Rhod-2 and simultaneous left ventric-

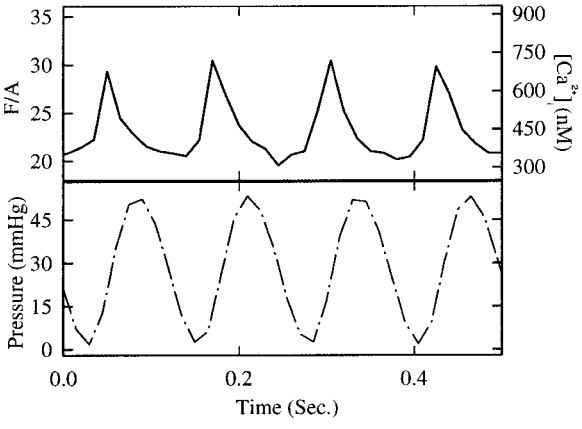

FIGURE 10 Calcium transients (*top*) represented by *F*/*A* (left *y* axis) or calcium concentration (right *y* axis) with simultaneous recording of left ventricular pressure (*bottom*).

ular pressure tracing from a perfused mouse heart. It clearly illustrates the upstrokes of the Ca^{2+}-transient during systole and decline during diastole, and that the calcium transient precedes the rise in left ventricular pressure. For a group of four perfused mouse hearts, the Ca^{2+}-transient signals represent 33 ± 9% of the diastolic fluorescence intensity. The $[Ca^{2+}]_i$ calculated values are 368 ± 68 nM and 654 ± 164 nM in diastole and systole, respectively.

DISCUSSION

The results presented here validate the use of fluorescence and absorbance measurements to quantitate Rhod-2 based measurements of intracellular calcium in the isolated perfused mouse heart. The proposed methodology has potential for other dyes that do not exhibit a fluorescence excitation or emission shift, but a change in quantum efficiency provided that the assumptions for our theoretical derivation are satisfied. Eq. 20 is accurate for quantifying the fluorescence-to-absorbance ratio of a fluorophore in scattering tissue if the tissue is homogeneous with nonreentrant geometry. It also requires that changes in tissue scattering at the excitation and detection wavelengths are nearly identical (i.e., $\Delta\mu_s'^{\lambda 1} \approx \Delta\mu_s'^{\lambda 2}$) and the measured reflectance $R^{\lambda 1} \approx R^{\lambda 2}$. The assumption of $\Delta\mu_s'^{\lambda 1} \approx \Delta\mu_s'^{\lambda 2}$ has been justified for $\lambda_2 - \lambda_1 < 100$ nm in the visible and NIR range by previous studies (Cheong et al., 1990), and is also confirmed for mouse heart tissue by our experimental results presented in Fig. 7. The requirement of $R^{\lambda 1} \sim R^{\lambda 2}$ was used in our experiment to further eliminate the influence of $\Delta\mu_s$ on the detection of the absorbance ratio of $A^{\lambda 1,\lambda 2}$, and was fulfilled by a proper selection of λ_1 and λ_2.

It has been known that the isosbestic wavelengths are useful for obtaining fluorescence and absorbance of a fluorophore and eliminating the interference of tissue filtration due to changes in oxygenation state (Brandes et al., 1994). λ = 524, 548, 568, and 589 nm are the four measured isosbestic points of mouse heart within the range of 500–600 nm. Anyone of the first three, which are sensitive to Rhod-2, can be selected for excitation, whereas 589 nm, which is insensitive, can thus be used for emission detection. 524 nm was chosen for excitation rather than 548 or 568 nm because our in vivo study on mouse heart tissue demonstrated that the quantum efficiency of fluorescence emission at 589 nm is higher if excited at 524 nm (see Fig. 2 *B*). Another reason for choosing 524 nm for excitation is that $R^{524} \sim R^{589}$. Fig. 6 *C* shows an example of comparison of the ratios $F^{524,589}/A^{524,589}$ and $F^{548,589}/A^{548,589}$, obtained from a perfused mouse heart during Rhod-2 washout. The underestimation of $F^{548,589}/A^{548,589}$ in the first 20 min was likely induced by a higher washout rate of $A^{548,589}$ than that of $A^{524,589}$. This is presumably because of the mismatch of spectral reflectance, or $\Delta R^{548,589}$ is higher than $\Delta R^{524,589}$, resulting in a higher offset related to any changes in μ_s' according to Eq. 12. Finally, changes in the heart oxygenation state at 548 nm are greater than at 524 nm, as indicated in Fig. 3 *B*. The change in optical density (OD) near 548 nm is much steeper than that near 524 nm, making 548 nm much more sensitive to changes in oxygenation than 524 nm.

A shortcoming of using Rhod-2 is that a measurement of F_{max} must be made on each heart. Previously, digitonin has been used to saturate Rhod-2 with calcium (Del Nido et al., 1998). Here we used cyclopiazonic acid and high calcium perfusate and compared this to digitonin. Similar results were obtained, however; the cyclopiazonic acid gave a much better steady-state F_{max} and there was little evidence of leakage of Rhod-2 and myoglobin, as occurs with digitonin. Errors in F_{max} will lead to errors in the value of $[Ca^{2+}]_i$ determined; for example, if F_{max} is underestimated, then the calculated $[Ca^{2+}]_i$ will be overestimated.

Calcium transient signals represent 33 ± 9% of diastolic fluorescence intensity. The calculated calcium concentration for perfused mouse heart were 368 ± 68 nM and 654 ± 164 nM in diastole and systole, respectively. These results agree well with those previously reported using microinjection of aequorin in the mouse heart (Hampton et al., 1998).

It is important to note that we have not determined subcellular localization of Rhod-2. Del Nido and colleagues have shown that Rhod-2 was located in the cytosol and that there was no evidence of mitochondrial deposition. However, other groups, such as Trollinger et al. (1997), have found predominant mitochondrial loading. This apparent discrepancy may be due to very different loading techniques. Nevertheless, we cannot exclude that a portion of the fluorescence is arising from mitochondria in this method.

In conclusion, we demonstrate on both theoretical and experimental grounds that measurement of quantum efficiency changes of Rhod-2 with calcium binding can be used to quantitate calcium concentration changes in the perfused mouse heart.

We acknowledge useful discussions with other members of the Center for Light Microscope Imaging and Biotechnology, and support from the National Science Foundation (MCB 8920118), National Institutes of Health (HL-40354, HL-02847, HL-03826), and American Heart Association (B98452P).

REFERENCES

Brandes, R., V. M. Figueredo, S. A. Camacho, A. J. Baker, and M. W. Weiner. 1993. Quantitation of cytosolic [Ca^{2+}] in whole perfused rat heart using Indo-1 fluorometry. *Biophys. J.* 65:1973–1982.

Brandes, R., V. M. Figueredo, S. A. Camacho, B. M. Massie, and M. W. Weiner. 1992. Suppression of motion artifacts in fluorescence spectroscopy of perfused hearts. *Am. J. Physiol. Heart Circ. Physiol.* 263: H972–H980.

Brandes, R., V. M. Figueredo, S. A. Camacho, and M. W. Weiner. 1994. Compensation for changes in tissue light absorption in fluorometry of hypoxic perfused rat heart. *Am. J. Physiol. Heart Circ. Physiol.* 266: H2554–H2567.

Chance, B. 1951. Rapid and sensitive spectrophotometry. III. A double beam apparatus. *Rev. Sci. Instrum.* 22:634–638.

Chance, B., H. Liu, T. Kitai, and Y. Zhang. 1995. Effects of solutes on optical properties of biological materials: models, cells, and tissues. *Anal. Biochem.* 227:351–362.

Cheong, W. F., S. A. Prahl, and A. J. Welch. 1990. A review of the optical properties of biological tissues. *IEEE J. Quant. Elec.* 26:2166–2185.

Del Nido, P. J., P. Glynn, P. Buenaventura, G. Salama, and A. P. Koretsky. 1998. Fluorescence measurement of calcium transients in perfused rabbit heart using rhod-2. *Am. J. Physiol. Heart Circ. Physiol.* 274: H728–H741.

Eason, G., A. Veitch, R. Nisbet, and F. Turnbull. 1987. The theory of the backscattering of light by blood. *J. Phys. D.* 11:1463–1479.

Efimov, I. R., B. Ermentrout, D. T. Huang, and G. Salama. 1996. Activation and repolarization patterns are governed by different structural characteristics of ventricular myocardium: experimental study with voltage-sensitive dyes and numerical simulations. *J. Cardiovasc. Electrophysiol.* 7:512–530.

Farrell, T. J., M. S. Patterson, and B. Wilson. 1992. A diffusion theory model of spatially resolved, steady-state diffuse reflectance for the noninvasive determination of tissue optical properties in vivo. *Med. Phys.* 19:879–888.

Field, M. L., A. Azzawi, P. Styles, C. Henderson, A-M. L. Seymour, and G. K. Radda. 1994. Intracellular Ca^{2+} transients in isolated perfused rat heart: measurement using the fluorescent indicator Fura-2/AM. *Cell Calcium* 16:87–100.

Flock, S. T., B. C. Wilson, and M. S. Patterson. 1987. Total attenuation coefficients and scattering phase functions of tissue and phantom materials at 633 nm. *Med. Phys.* 14:835–841.

Fralix, T. A., F. W. Heineman, and R. S. Balaban. 1990. Effects of tissue absorbance on NAD(P)H and Indo-1 fluorescence from perfused rabbit hearts. *FEBS.* 262:287–292.

Gmitro, A. F., F. W. Cutruzzola, M. S. Stetz, and L. I. Deckelbaum. 1988. Measurement depth of laser-induced tissue fluorescence with application to laser angioplasty. *Appl. Opt.* 27:1844–1849.

Grykiewicz, G., M. Poenie, and R. Y. Tsien. 1985. A new generation of Ca^{2+} indicators with greatly improved fluorescence properties. *J. Biol. Chem.* 260:3440–3450.

Hampton, T. G., I. Amende, K. E. Travers, and J. P. Morgan. 1998. Intracellular calcium dynamics in mouse model of myocardial stunning. *Am. J. Physiol. Heart Circ. Physiol.* 274:H1821–H1827.

Haugland, R. P. 1996. Handbook of Fluorescent Probes and Research Chemicals. Michelle T. Z. Spence, editor. Molecular Probe, Eugene, OR. 511–514.

Haworth, H. A., and D. Redon. 1998. Calibration of intracellular Ca transients of isolated adult heart cells labelled with fura-2 by acetoxymethyl ester loading. *Cell Calcium.* 24:263–273.

Ishimaru, A. 1978. Wave Propagation and Scattering in Random Media, Vol. 1. Academic Press, New York.

Jacques, S. L., C. A. Alter, and S. A. Prahl. 1987. Angular dependence of HeNe laser light scattering by human dermis. *Lasers Life Sci.* 1:309–333.

Koretsky, A. P., L. A. Katz, and R. S. Balaban. 1987. Determination of pyridine nucleotide fluorescence from the perfused heart using an internal standard. *Am. J. Physiol. Heart Circ. Physiol.* 22:H856–H862.

Liu, H., B. Beauvoit, M. Kimura, and B. Chance. 1996. Dependence of tissue optical properties on solute-induced changes in refractive index and osmolarity. *J. Biomed. Opt.* 1:200–211.

MacGowan, G. A., C. Du, J. P. Suhan, D. L. Farkas, and A. P. Koretsky. 2000. Rhod-2 based measurements of intracellular calcium in the perfused mouse heart: cellular and subcellular localization and response to positive inotropy. *J. Biomedical Opt.*, in press.

Miyata, H., H. S. Silverman, S. J. Sollott, E. G. Lakatta, M. D. Stern, and R. G. Hansford. 1991. Measurement of mitochondrial free Ca^{2+} concentration in living single rat cardiac myocytes. *Am. J. Physiol. Heart Circ. Physiol.* 261:H1123–H1134.

Parrish, J. A. 1981. New concepts in therapeutic photomedicine: photochemistry, optical targeting and the therapeutic window. *J. Invest. Dermatol.* 77:45–50.

Patterson, M. S., and B. W. Pogue. 1994. Mathematical model for time-resolved and frequency-domain fluorescence spectroscopy in biological tissues. *Appl. Opt.* 33:1963–1974.

Patterson, M. S., E. Schwartz, and B. C. Wilson. 1989. Quantitative reflectance spectrophotometry for the non-invasive measurement of photosensitizer concentration in tissue during photodynamic therapy. *Proc. SPIE.* 1065:115–122.

Potter, W. R., and T. S. Mang. 1984. Photofrin II levels by in vivo fluorescence photometry. *In* Porphyrin Localization and Treatment of Tumors. D. R. Doiron and C. J. Gomer, editors. Liss, New York. 177–186.

Richards-Kortum, R., R. P. Rava, M. Fitzmaurice, L. L. Tong, N. B. Ratliff, J. R. Kramer, and M. S. Feld. 1989. A one-layer model of laser-induced fluorescence for diagnosis of disease in human tissue: application to atherosclerosis. *IEEE Trans. Biomed. Eng.* 36:1222–1232.

Salama, G., R. Lombardi, and J. Elson. 1987. Maps of optical potentials and NADH fluorescence in intact working hearts. *Am. J. Physiol. Heart Circ. Physiol.* 252:H384–H394.

Trollinger, D. R., W. E. Cascio, and J. J. Lemasters. 1997. Selective loading of rhod-2 into mitochondria shows Ca^{2+} transients during the contractile cycle in adult rabbit cardiac myocytes. *Biochem. Biophys. Res. Commun.* 236:738–742.

van der Putten, W. J. M., and M. J. C. van Gemert. 1983. A modelling approach to the detection of subcutaneous tumours by haematoporphyrin-derivative fluorescence. *Phys. Med. Biol.* 28:639–645.

Wilson, B. C., and S. L. Jacques. 1990. Optical reflectance and transmittance of tissue: principles and applications. *IEEE J. Quant. Elec.* 26: 2186–2199.

Wilson, B. C., and M. S. Patterson. 1986. The physics of photodynamic therapy. *Phys. Med. Biol.* 31:317–360.

Wu, J., M. S. Feld, and R. P. Rava. 1993. Analytical model for extracting intrinsic fluorescence in turbid media. *Appl. Opt.* 32:3585–3595.

Yodh, A., and B. Chance. 1995. Imaging and spectroscopy using diffusing light. *Phys. Today.* 48:34–40.